JOINT EUROPEAN TORUS

JET–P(91)63

D.F.H. Start, V.P. Bhatnagar, G. Bosia, M. Brusati, M. Bures, D. Campbell, C. Challis, G.A. Cottrell, M. Cox[1], A. Edwards, L-G. Eriksson, P. Froissard, C. Gormezano, C. Gowers, S. Hugonard, J. Jacquinot, P. Kupschus, N. Gottardi, M.R. O'Brien[1], D. Pasini, F. Porcelli, E. Righi, F. Rimini, G. Sadler, D. Stork, A. Tanga, K. Thomsen, F. Tibone, B. Tubbing, M. von Hellermann and JET Team

Fast Wave Heating and Current Drive in JET: Present Results and Future Plans

Fast Wave Heating and Current Drive in JET: Present Results and Future Plans

D.F.H. Start, V.P. Bhatnagar, G. Bosia, M. Brusati, M. Bures, D. Campbell, C. Challis, G.A. Cottrell, M. Cox[1], A. Edwards, L-G. Eriksson, P. Froissard, C. Gormezano, C. Gowers, S. Hugonard, J. Jacquinot, P. Kupschus, N. Gottardi, M.R. O'Brien[1], D. Pasini, F. Porcelli, E. Righi, F. Rimini, G. Sadler, D. Stork, A. Tanga, K. Thomsen, F. Tibone, B. Tubbing, M. von Hellermann and JET Team*

JET-Joint Undertaking, Culham Science Centre, OX14 3DB, Abingdon, UK

[1]Culham Laboratory, Abingdon, Oxon, OX14 3DB
** See Appendix 1*

Preprint of Paper to be submitted for publication in the Proceedings of
IAEA Technical Committee Meeting on FWCD in Reactor Scale Tokamaks, Aries 1991

FAST WAVE HEATING AND CURRENT DRIVE IN JET : PRESENT RESULTS AND FUTURE PLANS

D F H Start, V P Bhatnagar, G Bosia, M Brusati, M Bures, D Campbell, C Challis, G A Cottrell, M Cox[1], A Edwards, L–G Eriksson, P Froissard, C Gormezano, C Gowers, S Hugonard, J Jacquinot, P Kupschus, N Gottardi, M R O'Brien[1], D Pasini, F Porcelli, E Righi, F Rimini, G Sadler, D Stork, A Tanga, K Thomsen, F Tibone, B Tubbing, and M von Hellermann,

JET Joint Undertaking, Abingdon, Oxon., OX14 3EA, UK

[1]Culham Laboratory, Abingdon, Oxon, OX14 3DB,UK

ABSTRACT A review is given of recent fast wave heating and current drive experiments on the JET tokamak. The heating studies encompass both minority cyclotron damping and direct electron absorption of the fast wave. In these experiments, a maximum power level of 22MW has been coupled to limiter plasmas. Bulk ion heating by minority ICRH has been demonstrated both in plasmas near the density limit and in pellet fueled H–mode discharges which reached a record thermal fusion product $n_d(0)\tau_e T_i(0) = 7.8\text{x}10^{20}\text{m}^{-3}\text{skeV}$. Electron heating by highly energetic minority tails appears to produce a saturation in the central electron temperature with increasing power per electron. Broadening of the heating profile by fast ion orbit effects could be the cause of this saturation. High quality H–modes have been produced with ICRF alone. With dipole phasing, τ_e values up to $2.8\tau_{goldston}$ have been obtained; with monopole phasing the enhancement factor over Goldston L–mode scaling is about 1.7. ^{3}He minority ions have been accelerated up to 1MeV tail temperature which is optimum for the ^{3}He–D fusion reaction and have produced 140kW of non–thermal ^{3}He–D fusion power. In high beta plasmas direct damping of the fast wave by combined TTMP and electron Landau damping has been observed. Current drive experiments include synergistic effects with LHCD, boostrap current with ICRF alone and minority ion current drive. The combination of LHCD and ICRH with monopole phasing produces an efficiency factor $\gamma = 0.4\text{x}10^{20}\text{m}^{-2}\text{A/W}$ due to damping of fast waves on the tail electrons generated by the LHCD. Up to 70% of the plasma current has been driven by the bootstrap current in 1MA, $\beta_p \simeq 2$ plasmas. The broadening of the current profile stabilises the sawteeth. Phasing the ICRF antenna currents at 90^0 has a dramatic effect on sawteeth when the minority resonance layer is near the q=1 surface. Normal sawteeth become monster sawteeth for $+90^0$ phase and are strongly destabilised for a phase of -90^0. An optimum power level is found for stability as expected from minority current drive theory.

1. INTRODUCTION

The ICRH system on JET consists of eight antennas distributed with approximately equal spacing around the torus. Each antenna has two vertical current straps which are fed by separate generators. The majority of experiments have been carried out with either zero (monopole) or π (dipole) phasing between the currents in these straps (heating mode). However, a recent innovation has been the introduction of a matching control system which allows any phasing to be imposed between these currents. As a result, directed waves can be launched for current drive studies. In this mode the strap currents are maintained at equal amplitude which causes the generators to supply different power levels to accomodate the cross coupling of power from one strap to the next. The difference in generator powers is reduced as the coupling resistance increases and is unimportant for $R_c \geq 4\Omega$. In both the heating and current drive modes, the matching is carried out automatically by two independent feedback loops controlling the frequency and stub lengths. In addition the coupling resistance can be kept constant by a plasma position control feedback which is essential to ensure continuous power to the plasma during H–mode experiments; without position control, R_c drops by a factor of two during the L–H transition and causes loss of power through generator tripping. With feedback on, the generators are completely unaffected by the transition. The plant parameters for each pulse are stored for future downloading into the system when similar matching conditions are encountered. As a result,

high powers can be achieved with the minimum of time spent on pre–tuning. Such a high level of automatic control is essential to interface eight antennas efficiently to the wide variety of magnetic configurations and plasma conditions that JET can generate. In this way the system has coupled 22MW into limiter discharges and has so far only been limited in X–point operation by the carbon or beryllium influxes from the X–point tiles.
In the present paper we review the progress in using fast waves for both heating and current drive in JET. The heating experiments described in section 2 include both direct damping on electrons and fundamental cyclotron absorption by minority ions; the latter have shown that bulk ion heating by minority ions can occur at sufficiently high plasma and minority densities. This is particularly important for next step devices since ion heating in high density plasmas provides the most efficient route to ignition[1]. ICRF is the only heating scheme that can provide this facility at present and on this basis a high minority density (D)T scheme has been proposed for NET/ITER[2].
In section 3 we present experiments dealing with various aspects of current drive with fast waves. Symmetrically injected waves have provided current drive through the bootstrap current and synergism with Lower Hybrid current drive. Directed waves have substantially affected sawtooth stabilisation when the minority resonance layer is placed close to the q=1 surface. Qualitative comparisons with theory suggest that these effects are the first evidence for minority ion current drive[3] which is predicted to be capable of strongly modifying the current density gradient near q=1 under these conditions[4].
Section 4 summarises the future plans for fast wave current drive on JET in both the near and long term.

2. FAST WAVE HEATING

Absorption of the fast magnetosonic wave can occur by three mechanisms, namely cyclotron damping, mode conversion, and a combination of electron Landau damping (ELD) and transit time magnetic pumping (TTMP). The mode conversion and ELD+TTMP processes allow power to be coupled directly to the electrons. Cyclotron damping puts power into minority ions at the fundamental cyclotron resonance or into the majority ions at harmonics of the cyclotron frequency. The majority of experiments carried out on JET use cyclotron damping by minority ions which, as shown in fig 1, can lead to either electron heating or majority ion heating depending, respectively, on whether the minority tail temperature T_t is greater than or less than the critical energy E_{crit}. The electron heating regime is most commonly used on JET since the ion heating regime requires somewhat restricted parameter space of high electron density together with high (typically >10%) minority concentration. However, with such high densities in pellet injection experiments and density limit studies there is evidence for bulk ion heating as described in section 2.1. It is particularly important to demonstrate this transfer of power to the bulk ions since it is a key feature of the ICRH scheme proposed for ITER[2]. That scheme uses 30% deuterium minority in a tritium plasma and calculations using the ICRDEP and JETTO codes[5] show that about 50% of the power goes to heat the ions. Moreover such calculations show that the auxiliary power required to reach ignition is substantially reduced by the use of an ion heating scheme. At present ICRH is the only available method for ion heating in a reactor since penetration considerations force neutral beam injection to MeV energies and into the electron heating regime. Section 2.2 presents a range of results in the minority ion/electron heating regime and section 2.3 summarises the results of ELD+TTMP direct electron damping experiments.

2.1 MAJORITY ION HEATING BY (H)D ICRH

Strong evidence for collisional power transfer from energetic minority hydrogen ions to deuterium majority ions has been obtained in high density discharges created either by pellet injection or by strong gas puffing. The deep pellet injection experiments produced improved central confinement of H–mode plasmas which resulted in a record thermal fusion triple products of $n_d(0)\tau_e T_i(0) = 7.8\text{x}10^{20}\text{m}^{-3}\text{skeV}$[6,7]. The gas puffing experiments were designed primarily to test the density limit which was found to depend more on the power reaching the plasma edge than on the usual Murakami parameter[8].

2.1.1 Pellet Enhanced Performance (PEP) in H–mode Plasmas.

Pellet injection into double null X–point discharges has allowed the creation of H–mode plasmas with the central thermal transport reduced by a factor of two[7]. On–axis H–minority ICRH has been used to heat these high performance plasmas with hydrogen concentrations of the order of 15% of the electron density. In order to avoid mode conversion at such high minority concentration, the RF antennas were phased in dipole mode. Typical time evolution of the plasma parameters is shown in fig.2. A 4mm pellet is injected at 5s and causes the central density, $n_e(0)$, to rise immediately to $1.5x10^{20}m^{-3}$. ICRH power is then applied (together with a small amount of neutral beam injection) and an H–mode is formed at 5.5s. The enhanced regime lasts until 6.2s. At this time the central electron and ion temperatures, $T_e(0)$ and $T_i(0)$ respectively, have reached 10 keV and the central density has a value $n_e(0)=7x10^{19}m^{-3}$. Note that even at this density the equipartition power is small compared with the ICRF input power density due to the high value of $T_e(0)$. Consequently, the fact that $T_i(0)$ is often equal to and sometimes exceeds $T_e(0)$, as in fig 3, suggests that the ion and electron heating rates are almost equal. This conclusion is confirmed by self consistent, combined full wave and Fokker–Planck calculations using the PION code[9] as shown in fig 4. The power from the minority to the bulk ions, P_{m-i}, exceeds the power from the minority to the electrons, P_{m-e}, by about a factor of two and is comparable with the sum of P_{m-e} and the direct electron heating, $(P_{eld}+P_{ttmp})$.

2.1.2 Density Ramp Experiments

These experiments were carried out in limiter discharges with $I_p=3MA$ and $B_t=3.1T$ in which on–axis H–minority ICRH was applied to the deuterium plasma. The density in the centre was ramped up to $8x10^{19}m^{-3}$ by strong gas puffing as shown in fig. 5. During the density rise, the central electron temperature decreased from 8keV to 4.5keV for a constant RF power input of 9.5MW. In contrast, the central ion temperature remained constant so that the bulk ion energy density in the plasma core increased by almost a factor of two as shown in fig. 6. This implies that a greater fraction of the ICRH was being delivered to the bulk ions in the high density regime. Again, PION code calculations confirm this deduction. The enhanced ion heating results from the reduced minority tail temperature which shows up as reduced fast ion energy content. In pulse 20307, the fast ion energy content (W_f) decreases by a factor of four during the density ramp. The PION code reproduces the time behaviour of W_f almost exactly. The strong reduction in W_f is a consequence of the sensitivity of the slowing down time to a simultaneous increase in n_e and a decrease in T_e. The calculated power transfer from the minority ions to the electrons and majority ions, P_e and P_i respectively, are shown in fig. 7. The value of P_i increases by about 40% during the pulse which is less than the twofold increase in $3/2n_i(0)T_i(0)$ (see fig 5). The difference could be due to both a peaking of the ion heating profile as the density increases (as predicted by the code), and an increase in the equipartition term in the plasma centre.

2.2 ELECTRON HEATING BY MINORITY IONS.

On–axis minority ICRH at the 10MW power level produces an absorbed power density of the order of $2MW/m^3$. Together with a minority concentration of typically 5% of n_e, a central density of $3x10^{19}m^{-3}$ and a central electron temperature of 10keV, this power density creates minority distributions with tail temperatures in the MeV range. The majority of JET experiments are carried out with the ICRF system operating in this regime in which the collisional power loss from the minority ions is predominantly to electrons. Examples of the results achieved include the scaling of $T_e(0)$ with RF power per electron, the production and heating of H–mode plasmas with ICRH alone, and the achievement of 140 kW of ^{3}He–D fusion power through the acceleration of ^{3}He minority ions with energies close to 1MeV.

2.2.1 Central Electron Temperature Scaling with $P_{rf}/n_e(0)$

ICRH experiments in 3MA plasmas with either H–minority or ^{3}He minority ions have produced the data shown in fig 8[10]. These points are taken during monster sawteeth to

obviate the problem of redistribution of the fast ions by sawteeth. For values of $P_{rf}/n_e(0)$ up to $3x10^{-19}MWm^3$ the central electron temperature scales linearly with power per electron. For higher values, $T_e(0)$ tends to saturate. Correlated with this effect is a similar tendency towards saturation of the fast ion energy content, as determined from the equilibrium and diamagnetic energy measurements. The open circles in fig 8 are points for which the power in the centre is estimated in ref 10 to be less than 70% of the input power. Also depicted in fig 8 are the values of W_f calculated on the basis of the central slowing down time. These values are typically twice as large as those obtained with due allowance for profiles of power density, $T_e(r)$ and $n_e(r)$. Nevertheless, they serve to illustrate the strong increase expected in W_f as progress is made towards higher values of $T_e(0)$. The rapid change in W_f is a result of the slowing down time scaling as $T_e^{1.5}/n_e$. Thus the saturation of $T_e(0)$ implies a reduction in the fast ion energy content in the plasma centre over and above that which is due to normal power deposition and plasma profile effects.
Such a reduction of fast ions in the plasma centre could be due to the effect of large fast ion orbits spreading the electron heating profile outside the range of the initial heating profile of the minority ions or it could due to velocity space instabilities driven by the anisotropy of the minority distribution function. A calculation[11] of the redistributed electron heating profile when orbit effects are taken into account is shown in fig 9. This calculation corresponds to I_p=3MA, B_t=3.1T, P_{rf}=8.5MW, $n_e(0)=3x10^{19}m^{-3}$ and $T_e(0)$=8keV.

2.2.2 H–modes with ICRH alone.

The introduction of beryllium Faraday screens on the RF antennas has reduced ICRF generated impurities to insignificant levels even with monopole phasing[12]. This improvement, together with a plasma position feedback system which maintains a constant coupling resistance, has allowed high quality H–modes to be achieved with ICRH alone[13]. An example is shown in fig 10 for I_p=3MA, B_t=2.8T in a double null X–point configuration. The ICRH used H–minority in a deuterium plasma and dipole phasing at a frequency of 42MHz which placed the minority cyclotron resonance on–axis. The double null configuration allowed the last closed flux surface to match the antenna curvature which gave good coupling for the fast wave. The H–mode is formed at 52.5s, as shown by the reduction in the Dα signal, and lasts for 1.3s. Throughout the H–mode phase the RF coupling resistance is kept constant by the position feedback which moves the plasma 1cm towards the antenna. Once formed, H–modes appear to be sustainable with only 1cm separation although their formation requires a minimum separation of about 2.5cm.
According to the diamagnetic loop, the stored energy in pulse 21906 reaches 6MJ of which about 1.3MJ is due to the fast ions. The confinement time for the thermal component is 0.7s which is twice the Goldston L–mode value[14] and is similar to values obtained with neutral beam injection at the same power level. A comparison of τ_e for RF, NBI and combined heating is shown in fig 11 for a plasma current of 3MA. All these heating methods produce similar performance. The large circular point is the pellet enhanced H–mode described in section 2.1.1 for which there is about a 25% increase in the global confinement due to the improved central confinement.
In general the H–modes with dipole antenna phasing are superior to those with monopole phasing. This point is shown in fig 12 where the stored energy is plotted against loss power. The data were selected to be as near to steady state as possible by restricting the energy rise rate to less than 30% of the input power. The highest value of W_{dia} is 2.8 times the Goldston L–mode value and was achieved with dipole phasing. With monopole phasing the performance is less good with the confinement being typically 35% smaller than that with dipole antennas. Also the H–mode threshold power is lower with dipole phasing, a typical value being 5MW for a toroidal field of 2.8T, compared with 8MW for monopole antennas under similar conditions. The D–D reaction rate also depends on the phasing with dipole giving about twice the yield obtained with monopole. The highest D–D reaction rate was $5.5x10^{15}$/s with dipole phasing which is about ten times[6] that achieved at the same power level in L–modes plasmas.
The poorer performance with monopole phasing is not due to greater impurity production. However, during the course of theoretical investigations into the cause of impurity production from the Faraday screens, it was discovered that monopole operation can

strongly influence the plasma edge through the formation of a convective cell[15]. This cell is generated as a result of sheath rectification of the RF electric field and can penetrate about 2cm into the plasma. Dipole phasing does not generate such a cell. The resultant edge modification could be responsible for the phase dependent performance.

2.2.3 ^{3}He–D Non Thermal Fusion Yield Experiments

The energetic minority tails achieved in high power ICRF heated plasmas allow significant fusion yields to be obtained from the $^3He + D \rightarrow {}^4He(3.7MeV) + p(14.6MeV)$ reaction. Such experiments have been carried out on JET during recent years and considerable improvement in the reactivity was obtained with beryllium rather than carbon coated walls and limiters, due to the enhanced deuterium concentration in the plasma centre[16]. These experiments have been extended to higher fusion power levels in 1990, mainly through optimisation of both the discharge parameters and the magnetic configuration. The highest reaction rates were obtained in 3.5MA L–mode plasmas with central ICRH. A double null configuration was used with power loading being shared between the limiter, the X–point tiles and the antenna protection tiles. The He minority density was controlled by gas puffing and by ^{3}He neutral beam injection, although the best results were found with gas puffing since the beam injection produced too high a ^{3}He concentration in the plasma core. In general the reaction rates were better than those achieved previously and a maximum fusion power of 140 kW was reached with 14MW of input power as shown in fig 13. A strong correlation between the fusion power and the fast ion energy content was also observed, as in previous experiments[17]. These results have been modelled by calculations based on the Stix anisotropic distribution[18] and have been shown to be close to the optimum yields which correspond to tail temperatures in the region of 1MeV.

2.3 DIRECT ELECTRON HEATING BY TTMP+ELD.

Direct damping of the fast wave by the combined processes of TTMP and electron Landau damping has been observed[19] in high beta hydrogen plasmas in JET. The experiments were carried out in 2MA double null X–point plasmas with the toroidal magnetic field set at either 1.3T or 1.4T. The RF frequency was 48MHz so that the only cyclotron resonance was the hydrogen second harmonic at a distance of 0.4m inside the magnetic axis. Thus the only damping mechanism for the fast wave in the plasma centre was TTMP +ELD. The plasma was heated by both RF and NBI to achieve central electron beta values around 1.5%. The direct electron heating power deposition profile was deduced from the electron temperature response to square wave RF power modulation. The results obtained from the ECE temperature diagnostic are shown in fig 14. The power deposition profile is centrally peaked and the total fraction of power damped on the electrons accounts for 22% of the input power. Full wave[9] and ray–tracing[20] calculations predict more peaked profiles but the fraction of power damped on the electrons agrees well with the observed value. Additional profile information was obtained from the soft X–ray cameras which received emission from a wider cross section of the plasma than that covered by the ECE diagnostic (see fig 15). Note that the damping is almost zero near the q=1 surface. A recent Hamiltonian treatment of the wave–particle interaction predicts such an effect as being due to insufficient overlap of the resonance zones in velocity space at the q=1 surface[21].

3. FAST WAVE CURRENT DRIVE

3.1 COMBINED LHCD AND ICRH

The two prototype Lower Hybrid launchers on JET have succeded in coupling up to 2.4MW of power to limiter plasmas. In this section we describe briefly how ICRH with symmetrically launched fast waves has been able to enhance the Lower Hybrid current drive performance: a more detailed account is given by Gormezano et al[22] at this meeting. The usual measure of LHCD efficiency is the quantity $\gamma = IR\langle n_e \rangle / P$. Values of γ are plotted in fig 16 against the volume average electron temperature $\langle T_e \rangle$ for both Lower Hybrid alone and combined LHCD + ICRH. In the case of the combined RF experiments the power used

for calculating γ was the LH power plus an estimate of the ICRH power damped on the fast electrons obtained from modulation experiments. Typically this was in the range 10%–20% of the coupled ICRH power, the remainder being absorbed by H–minority cyclotron damping. As shown in fig 16, the efficiency factor increases monotonically with $<T_e>$ at a faster rate than that predicted by the theory of Karney and Fisch[23] for the launched parallel wavevector spectrum. The less than predicted values of γ at low $<T_e>$ are not surprising since upshifts in the parallel wavenumber are expected under these conditions. Although such upshifts help to fill the spectral gap, they also cause LH power to be absorbed by low phase velocity electrons, therebye reducing the current drive efficiency. At the higher $<T_e>$ values the good efficiency in the combined LHCD and ICRH experiments is due to an enhanced electron tail to energies beyond those expected from the launched spectra. This can be seen from fig 17 which shows the bremstrahlung spectra radiated by the fast electrons. The examples shown compare the LHCD alone with combined RF results and include cases where zero loop voltage and full current drive were achieved. The plasma current in these experiments was either 0.4MA or 1.5MA and the ICRH was operated with monopole phasing which produces a parallel wavevector spectrum which is symmetric about zero and covers the range $-5m^{-1}$ to $+5m^{-1}$. In the LHCD alone case the 'photon' temperature ranges from 38keV for 1.7MW of LHCD power to 59keV for 2.3MW of power. With 3.1MW of ICRF added, this temperature increases to 140 keV which implies a much higher electron tail temperature than can be generated by the launched spectrum. Thus, the fast waves appear to damp on the fast electrons generated by the LHCD and drive these electrons to substantially higher energy. Note that no such enhancement is observed with dipole phasing of the ICRF antennas which does not launch waves with low parallel wavevectors. Although the exact nature of the damping mechanism (TTMP, ELD or mode conversion) has yet to be determined, it is clear that this synergetic effect underlies the high values of γ in fig 17.

3.2 BOOTSTRAP CURRENT WITH ICRH ALONE.

These experiments aimed to demonstrate the existence of a bootstrap current in the absence of central particle fuelling. The absence of NBI heating also simplified the analysis since the bootstrap current was the only non–inductive current present. The experiments were carried out in double null X–point deuterium discharges with I_p=1MA, B_t=2.8T. The ICRH used dipole phasing at a frequency of 42.7MHz which placed the resonance close to the magnetic axis after allowance was made for the considerable Shafranov shift ($\simeq$ 0.35m); the poloidal beta in these plasmas was typically $\beta_p \simeq 2$. The evolution of the discharge with the highest bootstrap current is shown in fig 18. During the initial 1.5s of RF heating substantial ELM activity is generated and the low particle confinement clamps the line integral density at $4x10^{19}m^{-2}$. The discharge then switches to an ELM–free H–mode at 51.3s whereupon the improved energy and particle confinement times lead, respectively, to an increase in stored energy and a continuing density rise until the end of the H–mode at 53.0s. The behaviour of the surface loop voltage (V_l) reveals the presence of a substantial bootstrap current as shown in fig 19. At the end of the H–mode phase with ELMS, V_l goes negative and then recovers towards zero as current diffusion takes place. When the ELMS disappear a further reduction in V_l takes place followed by a slower return towards steady state. Also shown in fig 19 are the V_l traces calculated from a poloidal field diffusion code[24] on the basis of 1) both a change in resistivity and the presence of a bootstrap current, and 2) only a change in the plasma resistivity due to a change in T_e. The combination of resistivity reduction and bootstrap current produce a loop voltage response which shows good agreement with the experiment. During the ELM–free phase the predicted bootstrap current is of the order of 0.7MA. The time evolution of this current is shown in fig 20. During the period of high bootstrap current the sawteeth are suppressed as can be seen from the central electron temperature trace in fig 18. This is consistent with strong current profile broadening.

3.3 SAWTOOTH CONTROL BY ICRH PHASING

In 1981 Fisch proposed that non–inductive current could be driven by minority ion cyclotron heating with directed fast waves[3]. Subsequently, detailed bounce average Fokker–Planck calculations[4] showed that this scheme could be used to modify the current density profile,

and particularly the current density gradient, at the q=1 surface, thereby offering the possibility of controlling sawteeth. With the development of a system to phase the ICRF antennas on JET, experiments have been carried out to investigate the effects on the sawteeth of launching directed fast waves. The parallel wavevector spectrum for 90^0 phasing of the current straps[25] is compared in fig 21 with the usual dipole and monopole spectra. The studies were carried out in 2MA deuterium limiter discharges with hydrogen minority ions. The RF frequency was 42.7MHz and the magnetic field on axis was 2.6T which placed the hydrogen minority resonance tangential to the sawtooth inversion radius inside the magnetic axis as shown in fig 22. The misalignment between the inversion surface and the flux surfaces in fig 22 is due to a small difference in the plasma positions given by the soft X–ray tomography and the equilibrium calculation. With the resonance in this position, phasing the antenna current straps in dipole mode ($\phi = 180^0$) produced large sawteeth with a period(τ_{st}) of 0.2s as shown in fig 23 before 16sec. Changing the phasing to $+90^0$ to launch directed fast waves had a stabilising effect and increased the sawtooth period to 0.5sec which resulted in a saturation of the central electron temperature at the top of the sawteeth. Reversing the toroidal direction of the waves by applying -90^0 phase had a dramatic de–stabilising effect which produced very small sawteeth of short period (τ_{st}=30ms) as shown in fig 23. The electron temperature profiles corresponding to the $+90^0$ and -90^0 phases are shown in fig 24. In the de–stabilised case the profile is flattened at a level correponding to the crash of the large sawteeth obtained with $\phi = +90^0$.
A scan in ICRF power was carried out with $+90^0$ phase to determine the limits of the stabilising effect. The results are shown in fig 25. Monster sawteeth are generated at a power of only 2.8MW and are sustained for power levels up to 5MW. However, at more than 5MW the sawtooth period decreases with increasing power. This effect is illustrated in fig 26 which shows the timescale of the longest sawtooth produced within the RF pulse plotted against both the coupled power and the fast ion energy content; the latter is proportional to the average energy of the minority ions for constant minority concentration within the heating zone.
In contrast to the above effects of phasing with off–axis heating, phasing with on axis ICRH has little or no effect on sawteeth; similar monster sawteeth are produced by central ICRH regardless of the phase between the current straps.
Recent theoretical work (see ref. 26 and other references therein) has shown that monster sawteeeth could be due to the stabilisation of internal kink modes by fast ion pressure, provided this pressure is peaked well inside the q=1 surface, as is the case with on–axis ICRF heating. With off–axis ICRH, the modification of the local magnetic shear near the q=1 surface may play the most important role. An analysis of the direction of the wave relative to the plasma current shows that with $+90^0$ phase, and the resonance on the high field side of the magnetic axis, the current density gradient should be reduced at the q=1 surface, leading to a lengthening of the sawtooth period. In ref 27. a critical threshold value of the q=1 magnetic shear was proposed for the onset of the sawtooth crash in discharges where the fast ion pressure is not significant. A fair correlation was obtained between the sawtooth period and the resistive evolution time of the local shear from an initial low value, at the bottom of the sawtooth ramp, to this critical threshold value. An extension of this model is in progress to include ICRF waves with $\pm 90^0$ phasing applied to the q=1 surface.
The results of the power scan are also consistent with the hypothesis that minority current drive is at work. The production of a very high energy tail in perpendicular energy is expected to reduce the driven current both by accelerating more ions into trapped orbits and by allowing the slowing down process to be dominated by collisions with electrons. The current drive relies on ion–ion collisions and, in particular, the dependence of the ion–ion collision frequency on minority energy.

4. FUTURE PLANS

In the present operating period of JET a detailed study of the phasing effect on sawteeth will be undertaken in order to establish whether or not minority ion current drive is the underlying mechanism. For example the theory predicts that the current driven with the resonance tangent to the outboard q = 1 surface will be much smaller than for the inboard resonance due to the enhanced trapping of the minority ions. In this case, the phase required

for stability will be -90^0 rather than $+90^0$. Also theory predicts that with He minority ions the current can be made to reverse direction if Z_{eff} is less than 2. Applications for this method of current profile control will be sought in the form of switching sawteeth on or off and of stabilising mhd at q=2 such as locked modes due to error fields which eventually give rise to disruptions. A particularly attractive aim is to use minority current drive, rather than the central cooling due to the pellet injection, to produce the shear reversal which is observed to correlate with the enhanced confinement in PEP + H–mode plasmas[28].
After the shutdown to install the pumped divertor, the ICRF system will use new A2 antennas designed to match the single null configuration. The antenna geometry will be re–arranged into four groups of four striplines and the control system will be modified to suit this new arrangement. A diagram of one of these groups is shown in fig 27. It will be possible to apply any chosen phase within and between each group. In this way a peak directivity of 80% can be achieved. The present phase control maintains equal currents in the antenna by demanding different power levels from the supplying generators. At coupling resistances $R_c \lesssim 4\Omega$, this means that the system delivers considerably less than the maximum power. In the A2 configuration power will be circulated between the end striplines in each set of four, thereby enabling all the generators to reach maximum output. This advanced facility combined with the full 12MW LHCD installation, will provide a powerful tool for developing TTMP and synergistic current drive scenarios.

5. SUMMARY

Fast wave heating experiments on JET have explored all the scenarios depicted in fig 1. Heating of the majority ions by collisional power transfer from accelerated minority hydrogen ions has been observed in high density PEP+H–mode and density limit experiments. In the PEP+H studies the ion temperature sometimes exceeded the electron temperature and a record thermal triple product of $7.8 \times 10^{20} keVm^{-3}s$ was achieved together with a D–D reaction rate of $2 \times 10^{16} s^{-1}$.
Electron heating by collisions with very energetic minority ions in the MeV range is the usual heating scenario in JET due to the high coupled power (up to 22MW) and the low minority density (typically 5%) used to avoid dilution of the deuterium. With such energetic minority ions the central electron temperature tends to saturate with increasing power per electron. This could be due to the large orbits followed by these minority ions or it could arise from expulsion of energetic ions from the centre by velocity space instabilities driven by the large and highly anisotropic fast ion pressure.
High quality H–modes are produced with ICRH alone with dipole phasing and reach confinement times up to 2.8 times the Goldston L–mode value. With monopole phasing the performance is less good(1.7 times the Goldston confinement) and the power threshold for H–mode formation rises from about 5MW to around 8MW.
Optimisation of the minority tail temperature to around 1MeV in ^3He–D fusion experiments has produced 140 kW of fusion power for an input of 14MW of RF power. The maximum Q value obtained in these experiments was 1.2% at power levels in the range 10MW to 12MW. Direct damping of the fast wave on electrons by the combined action of TTMP and electron Landau damping has been seen in discharges with an electron beta value of 1.5%.
Current drive with fast waves has been studied in the areas of synergism with Lower Hybrid current drive, bootstrap currents with ICRF alone and antenna phasing effects on the stability of sawteeth. With ICRH coupled to plasmas in which a large fraction of the current is driven by LHCD, the current drive efficiency and the fast electron tail temperature are substantially increased when the antennas have monopole phasing. Driven currents up to 1.5MA have been achieved. The usual efficiency figure of merit reaches a value $\gamma = 0.4 \times 10^{20} m^{-2}A/W$ taking into account the power from the fast waves coupled to the electron tail.
The bootstrap current has contributed up to 70% of the plasma current in 1MA H–mode plasmas which were heated to poloidal beta values of two by ICRF alone. Thus the bootstrap current can reach substantial values also in the absence of a central particle source.
Phasing the ICRF antennas to launch travelling waves has a dramatic effect on the sawteeth when the cyclotron resonance layer is tangential to the q=1 surface on the high field side of

the magnetic axis. With $+90^0$ phasing between current straps, the sawtooth period is prolonged; with -90^0 phasing the sawteeth are de–stabilised to become shorter and of smaller amplitude than those in the ohmic phase of the discharge. Maximum effect is achieved at relatively low power levels ($\simeq$ 4MW). At higher power levels the stabilising effect of $+90^0$ phasing diminishes. These results are qualitatively consistent with modification of the current density gradient by the minority current drive mechanism first proposed by Fisch.
In the future, a new set of antennas are planned for the pumped divertor phase of JET. These antennas will give a good match to single null X–point plasmas and provide improved directivity for fast wave and combined ICRH and LH current drive

REFFERENCES

1) R Koch et al., Plasma Physics and Contr. Fusion Research, IAEA, Washington, 1990, paper CN–53 G–2–9.
2) J Jacquinot and the JET Team, Plasma Physics and Contr. Fusion 30(1988)1467.
3) N J Fisch, Nuclear Fusion 21(1981)15
4) M Cox and D F H Start, 1987 International Conference on Plasma Physics, Kiev, 1(1987)232.
5) C H Sack and A Taroni, private communication.
6) B Tubbing et al., Nuclear Fusion 31(1991)839.
7) P Kupschus et al., 18th EPS Conference. on Controlled. Fusion and Plasma Physics, Berlin 1991.
8) P Smeulders and the JET Team, 13th IAEA Conf. on Plasma Physics and Controlled Nuclear Fusion Research, Washington DC, USA, 1(1990)219.
9) T Hellsten and L–G Eriksson, JET report JET–P(89)65.
10) J G Cordey et al., 18th EPS Conference on Controlled Fusion and Plasma Physics, Berlin, 1991.
11) G A Cottrell, E Righi and D F H Start, to be published.
12) M Bures et al, Journal of Nuclear materials, 176 &177(1990)387
13) V P Bhatnagar et al., 18th EPS Conference on Controlled Fusion and Plasma Physics, Berlin 1991.
14) R J Goldston, Plasma Physics and Controlled Fusion 26, 1A(1984)87.
15) D D'Ippolito et al., Sherwood Fusion Theory Conf., Seattle(1990), to be published.
16) D F H Start and the JET Team, 13th IAEA Int Conf. on Plasma Physics and Controlled Nuclear Fusion Research, Washington DC, USA, 1(1990)679.
17) G A Cottrell, private communication.
18) J Jacquinot and G Sadler, JET Report JET–P(91), to be published in Fusion Energy and Design.
19) D F H Start et al., Nuclear Fusion 30(1990)2170.
20) V P Bhatnagar, et al., Nuclear Fusion 24(1984)955.
21) A Becoulet et al., 13th IAEA Int. Conf. on Plasma Physics and Controlled Nuclear Fusion Research, Washington DC, USA, 1(1990)811.
22) C Gormezano et al., IAEA Technical Committee Meeting on Fast Wave Current Drive in Reactor Scale Tokamaks, Arles, France 1991.
23) C F F Karney and N J Fisch, Physics of Fluids 28(1985)116.
24) C Challis, private communication.
25) V P Bhatnagar et al., 9th Topical Conf. on Radiofrequency Heating Power in Plasmas, Charleston, USA, 1991.
26) F Porcelli, 18th EPS Conference on Controlled Fusion and Plasma Physics, Berlin 1991, to be published in Plasma Physics and Controlled Fusion.
27) F Porcelli et al., JET report JET–R(88)16
28) M Hugon et al., submitted to Nuclear Fusion.

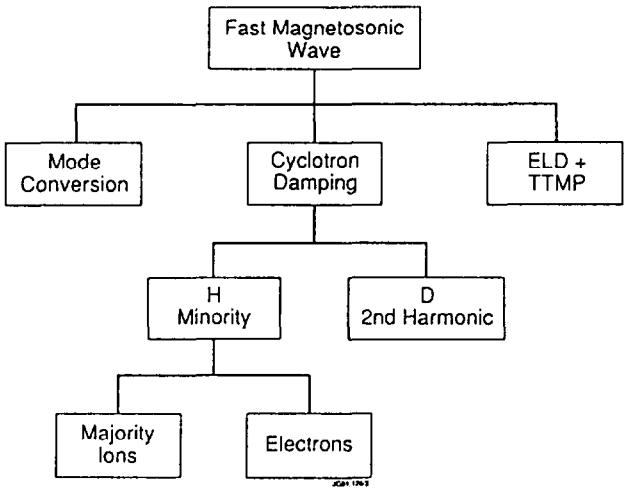

Fig. 1 Absorption mechanisms for the fast wave and power transfer routes.

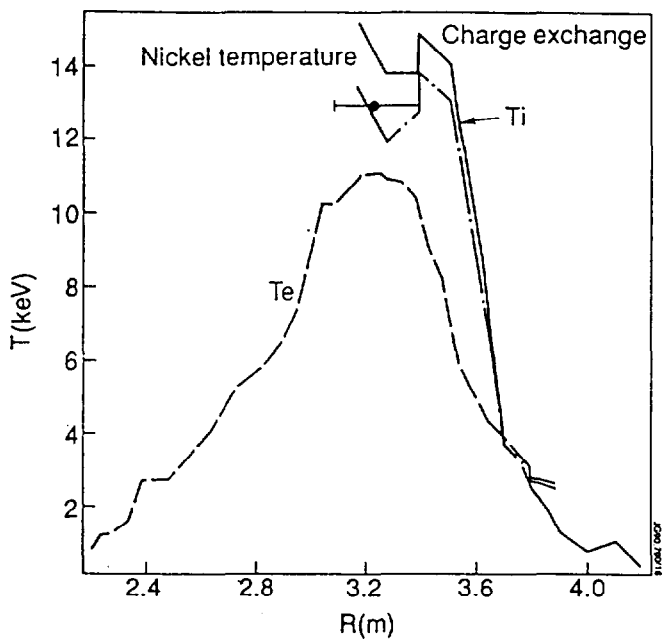

Fig.3 Electron and ion temperature profiles during PEP + H phase with $T_i(0) > T_e(0)$.

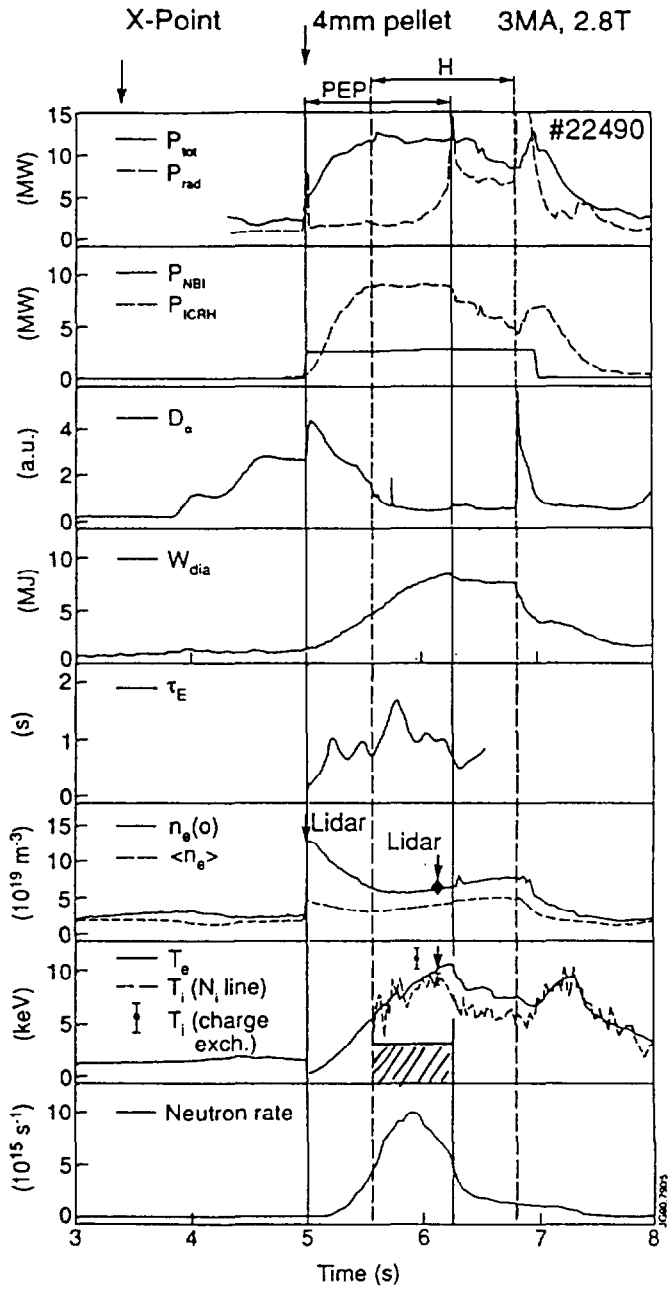

Fig.2 Plasma parameter evolution during the PEP + H–mode discharge for which $n_d \tau_e T_i \simeq 8 \times 10^{20} m^{-3} skeV$.

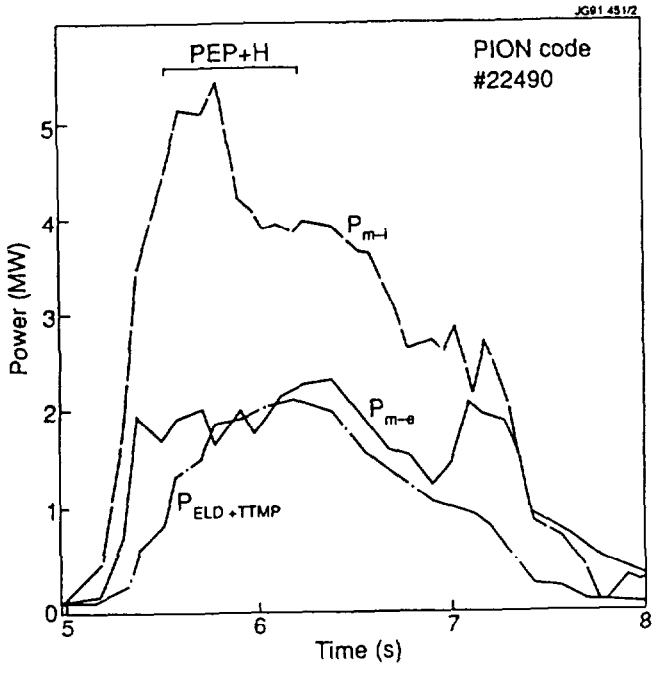

Fig.4 PION code results for minority and direct electron heating rates for pulse 22490.

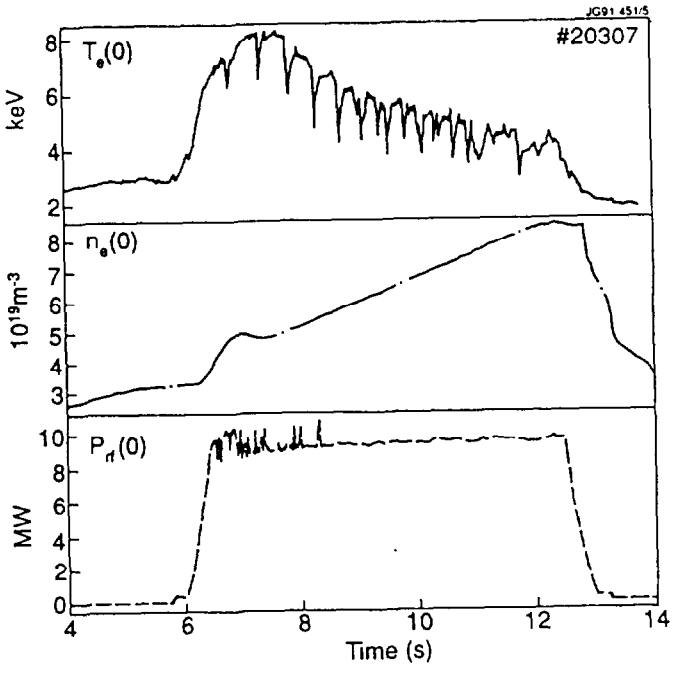

Fig.5 Central temperature and density evolution during density ramp experiments.

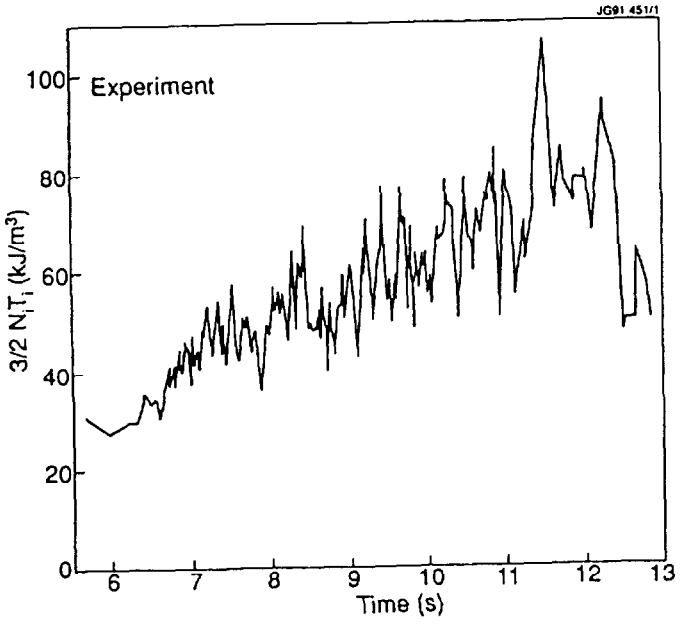

Fig.6 Central energy density of deuterium majority ions for pulse 20307.

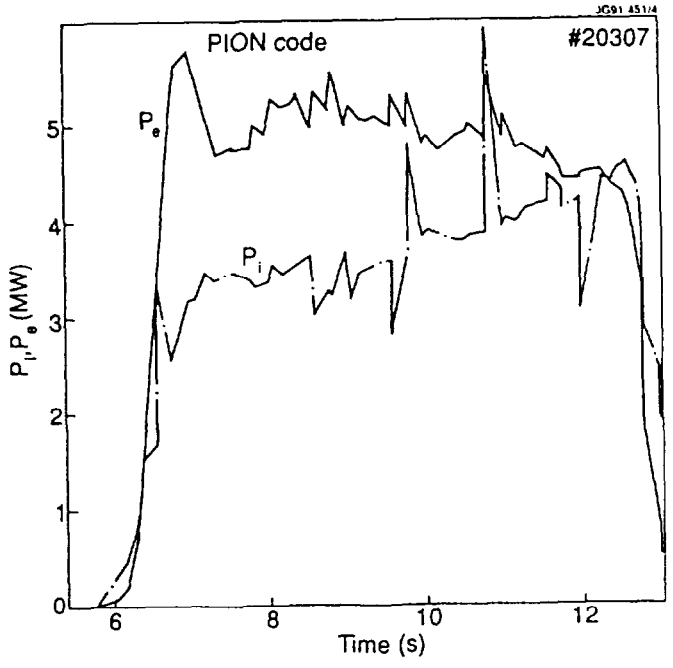

Fig.7 PION code results for ion and electron heating rates due to H–minority ions.

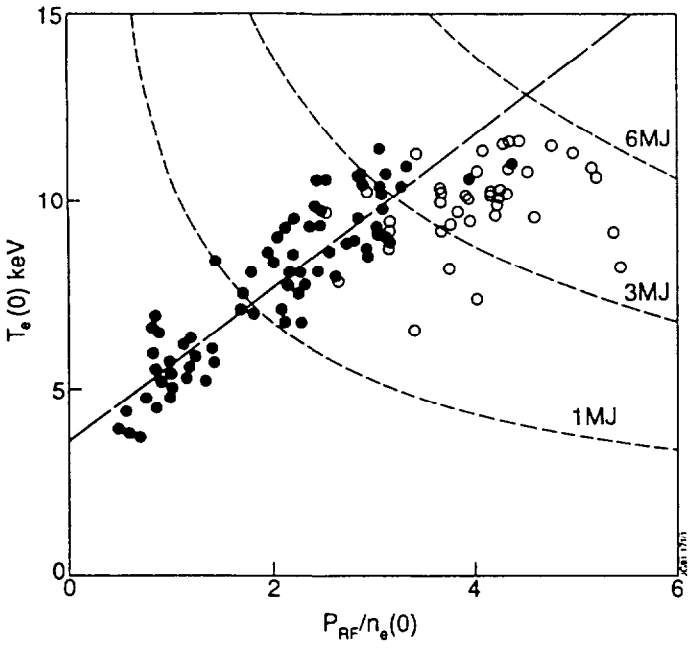

Fig.8 Central electron temperature versus $P_{rf}/n_e(0)$ for sawtooth–free plasmas.

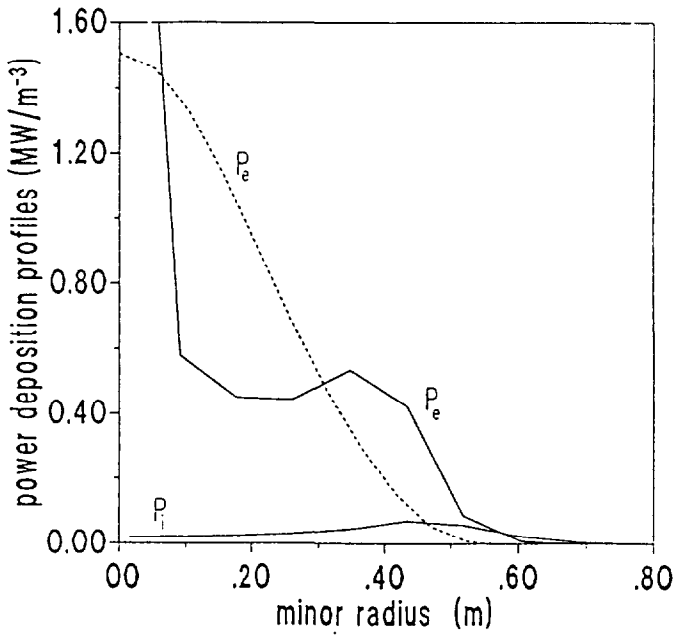

Fig.9 Electron heating power profile P_e with (full curve) and without (dashed) orbit effects.

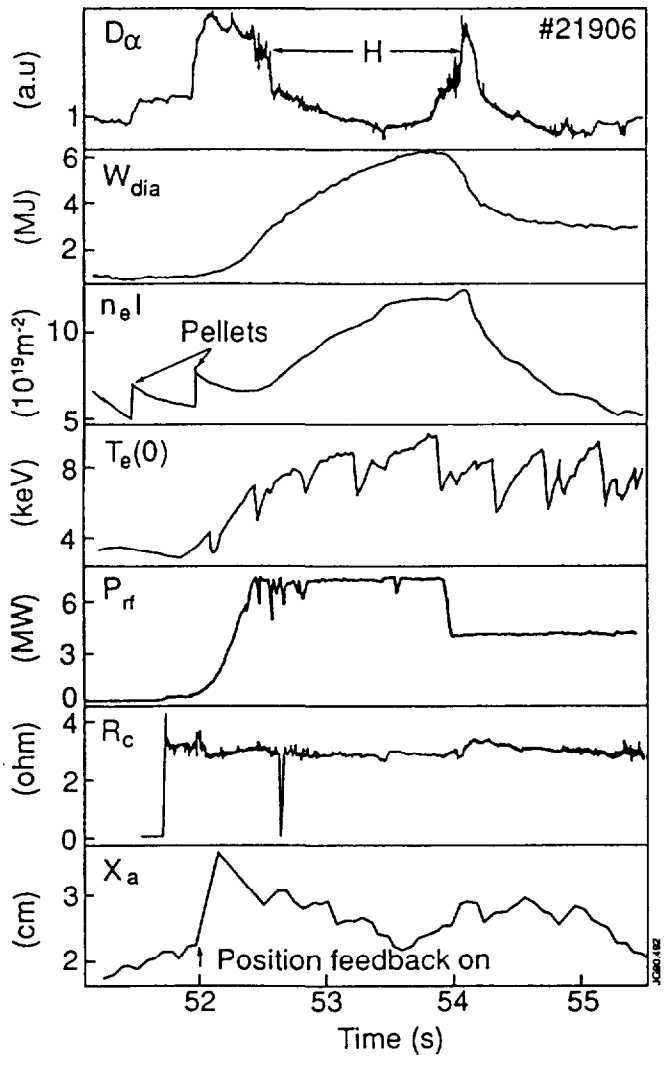

Fig.10 Plasma parameters during H–mode with ICRF alone.

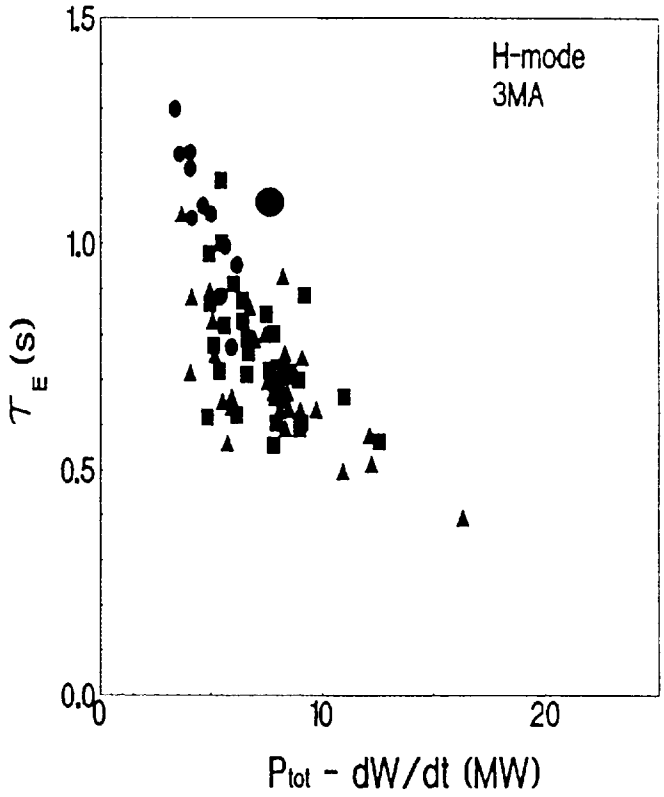

Fig.11 H–mode confinement for various heating methods: circles denote RF (the large circle with pellet injection), triangles denote NBI and squares are NBI + RF.

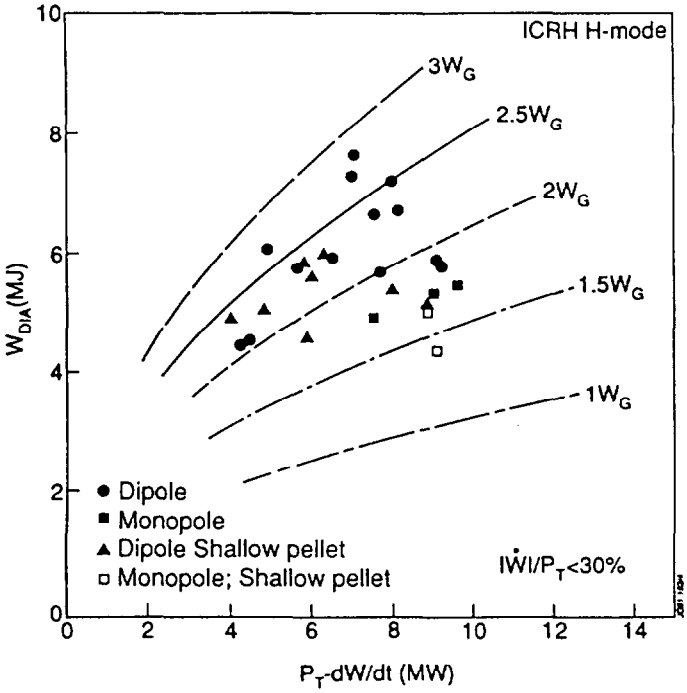

Fig.12 H–mode stored energy versus loss power.

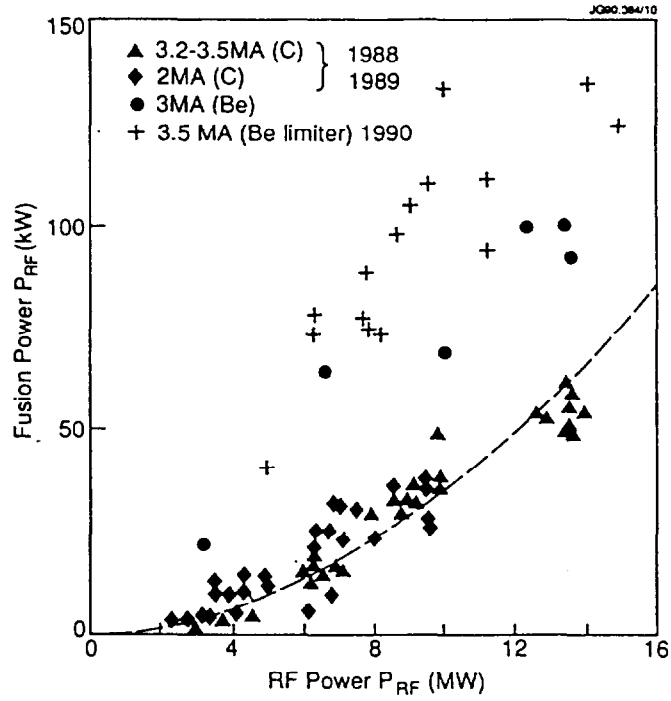

Fig.13 ^{3}He–D fusion power versus P_{rf}.

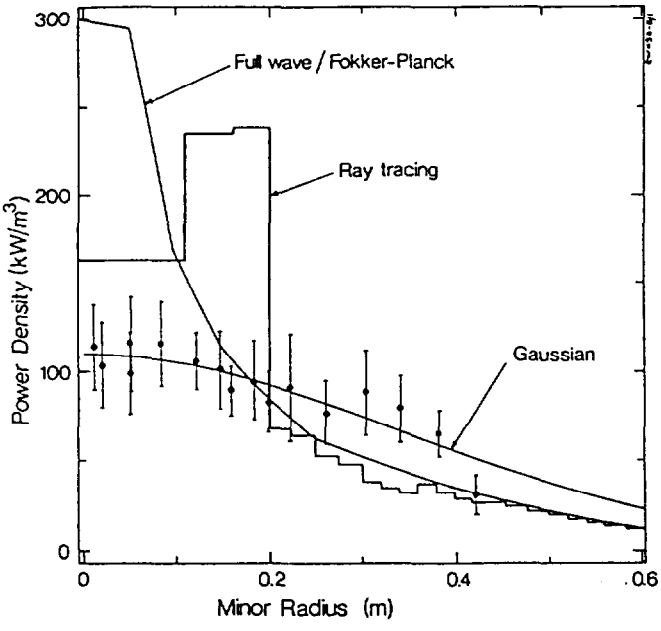

Fig.14 Direct electron heating profiles from ECE measurements compared with theoretical predictions.

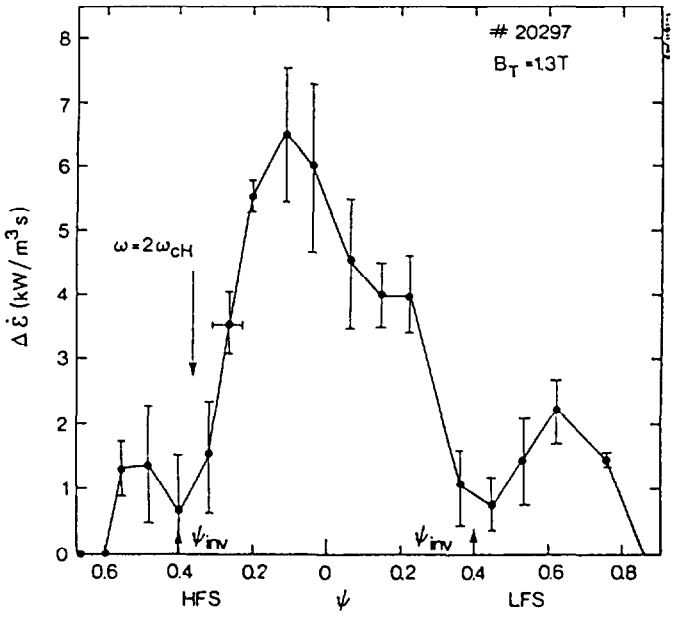

Fig.15 Increment in the rate of change of soft X–ray emission due to RF power modulation

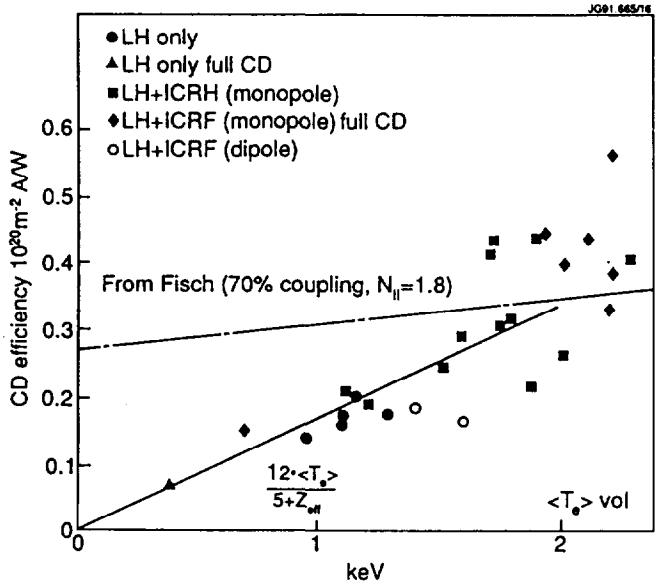

Fig.16 LHCD efficiency γ versus $<T_e>$ for LH and LH + ICRF.

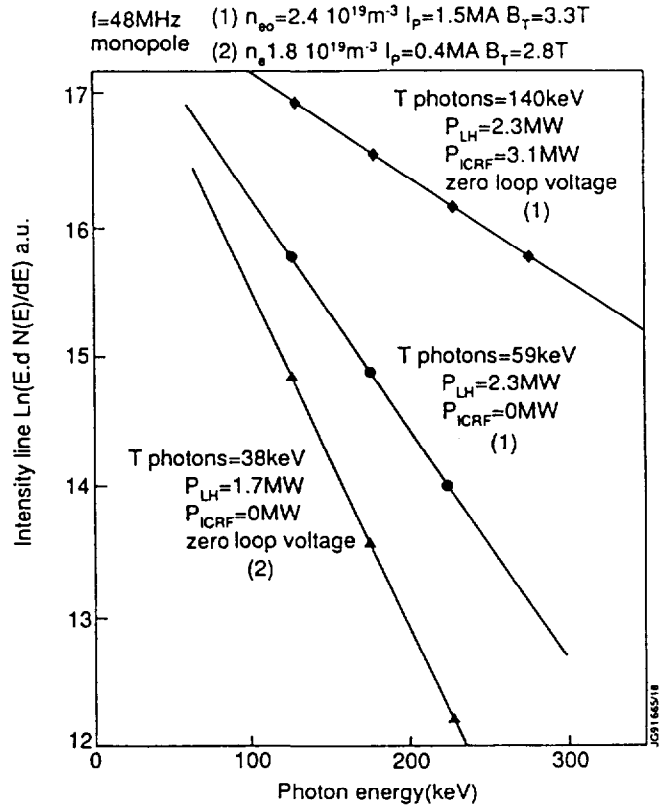

Fig.17 Bremstrahlung spectra from fast electrons driven by LHCD and LHCD + ICRF.

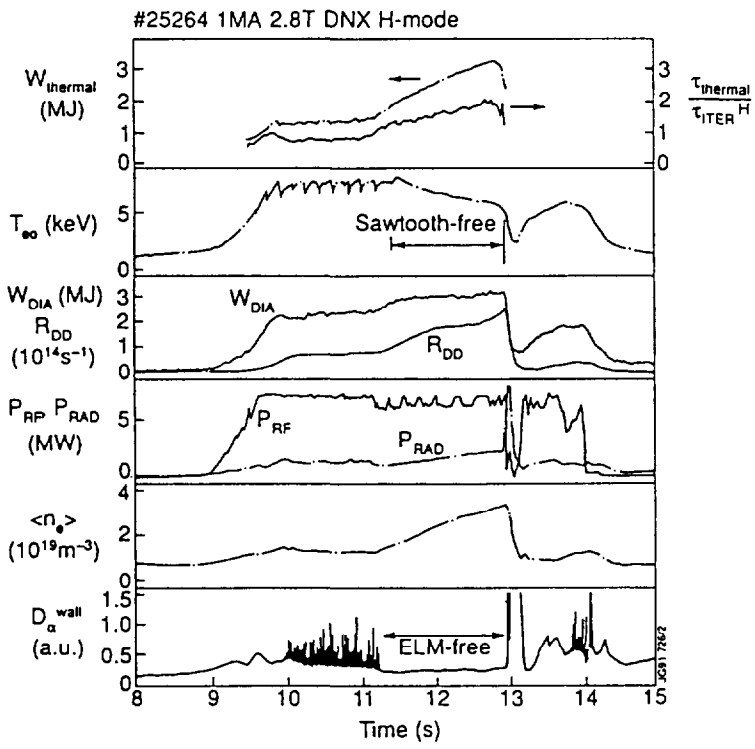

Fig 18 Plasma parameters during bootstrap current studies with ICRF alone.

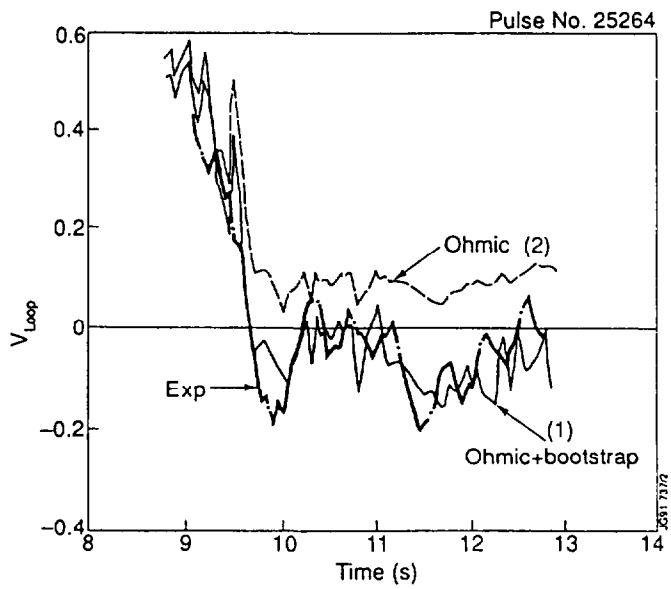

Fig.19 Experimental and theoretical surface loop voltage traces.

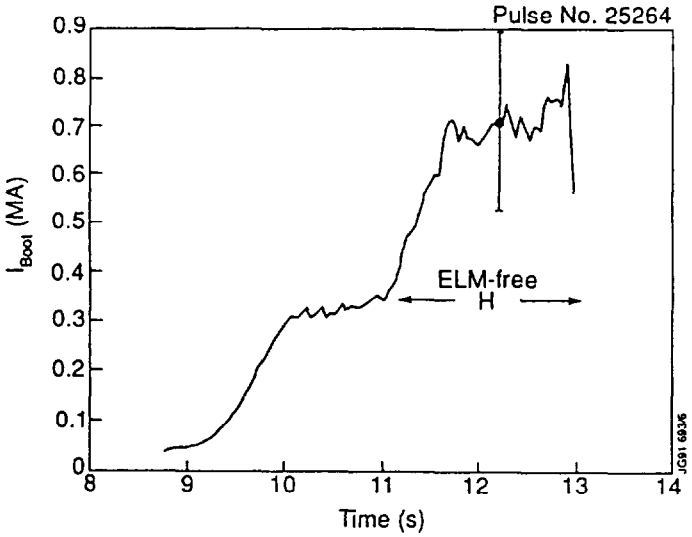

Fig.20 Time evolution of the predicted bootstrap current.

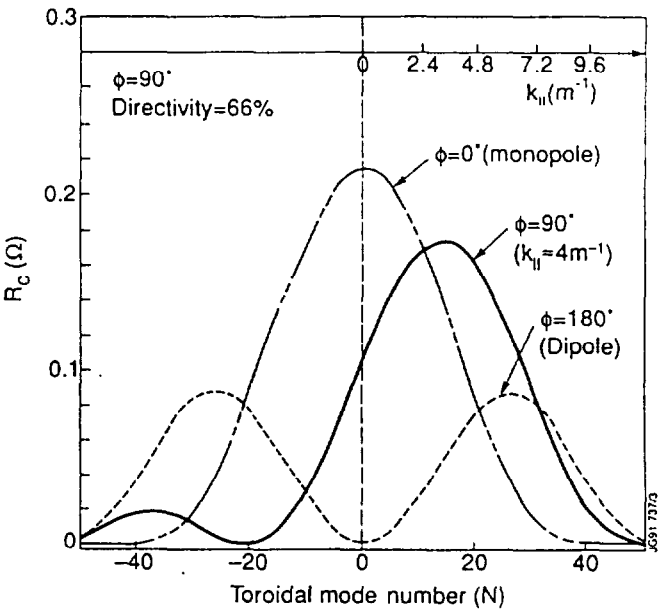

Fig.21 Parallel wavevector spectra for $\phi = 0^0$, $\phi = 90^0$ and $\phi = 180^0$ phasing.

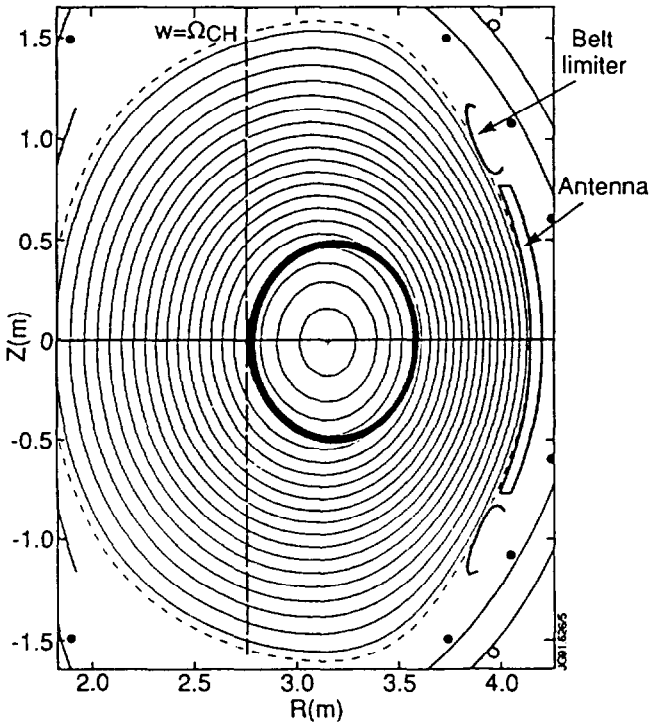

Fig.22 Magnetic configuration for sawtooth control by ICRF phasing.

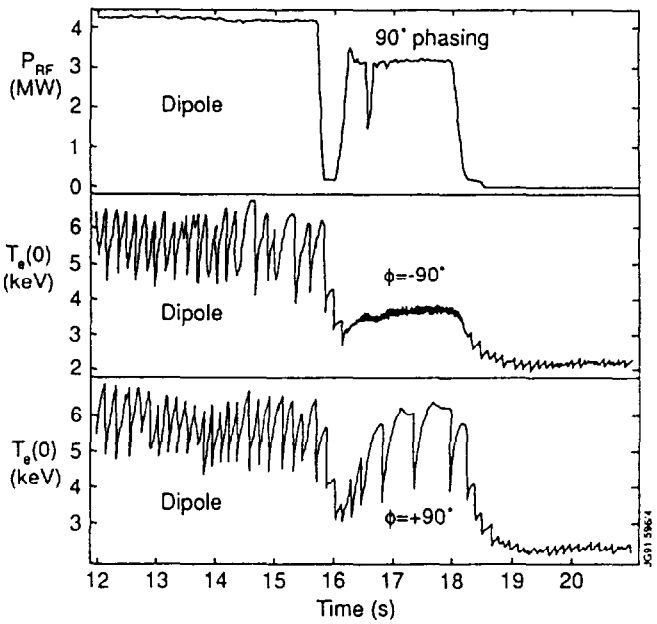

Fig.23 Effect of directed fast waves on sawtooth stability.

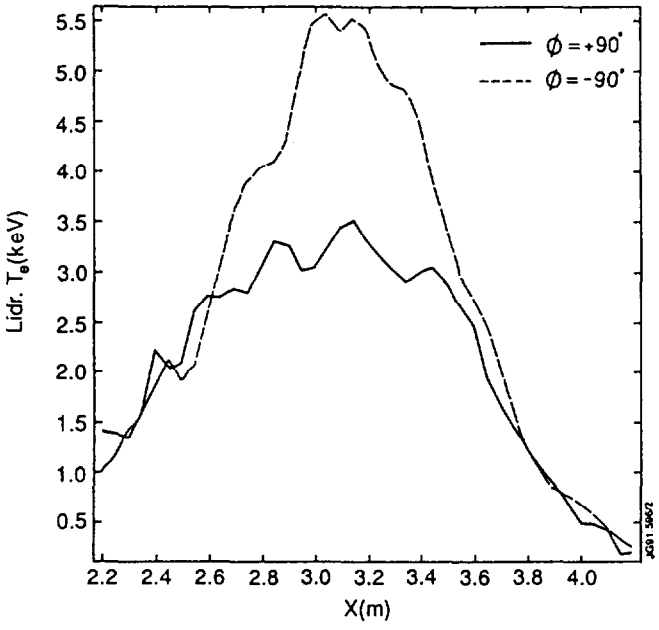

Fig.24 Electron temperature profiles for $\phi = +90^0$ and $\phi = -90^0$.

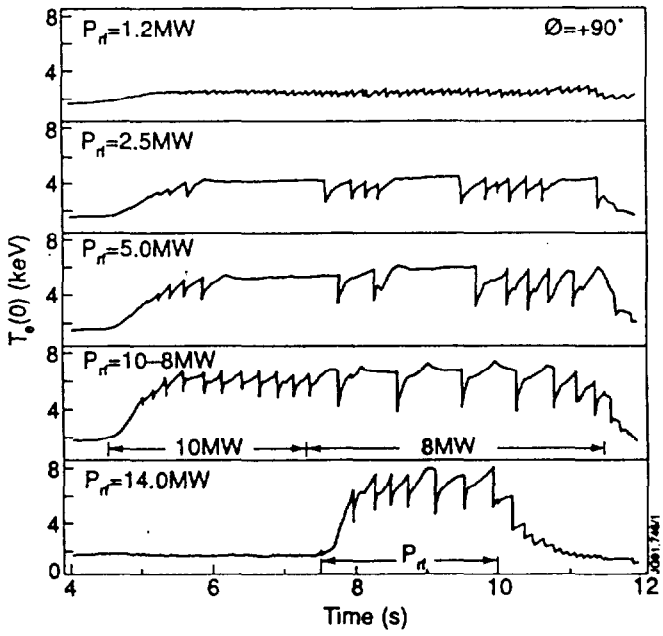

Fig.25 Sawtooth behaviour for $\phi = +90^0$ and various RF power levels.

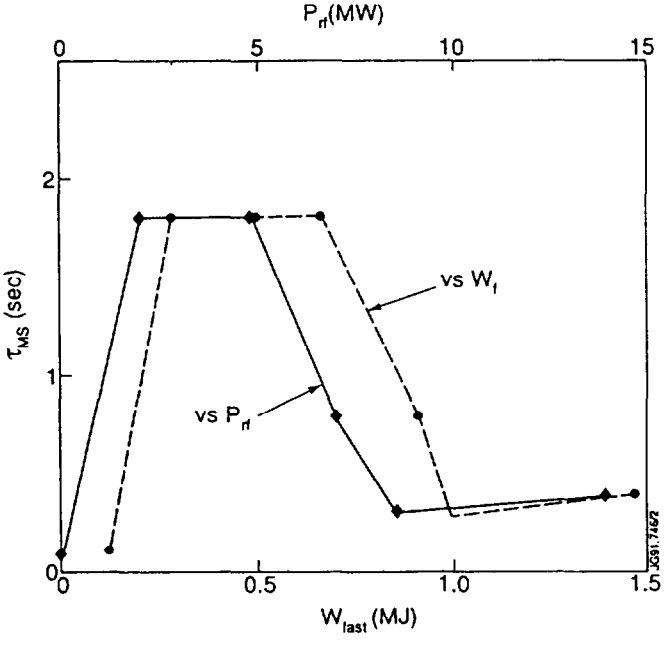

Fig.26 Maximum sawtooth period versus P_{rf} and W_f for $+90^0$ phasing.

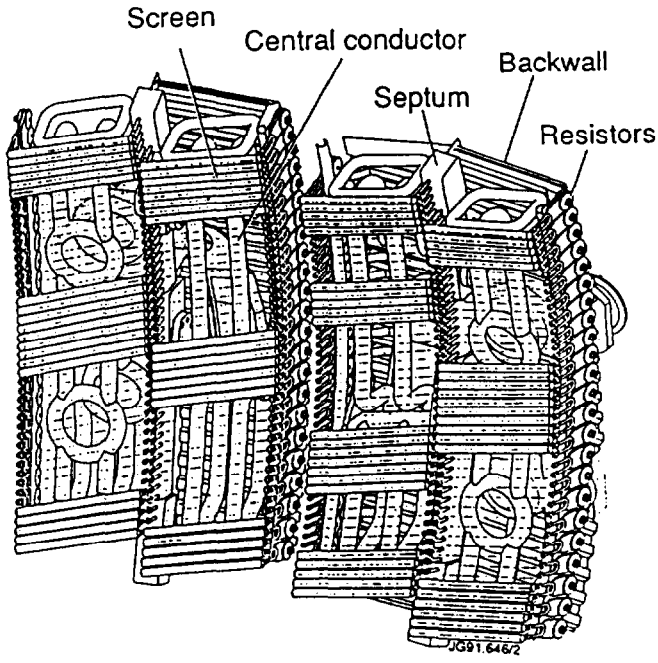

Fig.27 One unit of the A2 antenna array consisting of four phased current straps.

Appendix I

THE JET TEAM

JET Joint Undertaking, Abingdon, Oxon, OX14 3EA, U.K.

J.M. Adams[1], H. Altmann, A. Andersen[14], P. Andrew[18], M. Angelone[29], S.A. Arshad, W. Bailey, P. Ballantyne, B. Balet, P. Barabaschi, R. Barnsley[2], M. Baronian, D.V. Bartlett, A.C. Bell, I. Benfatto[5], G. Benali, H. Bergsaker[11], P. Bertoldi, E. Bertolini, V. Bhatnagar, A.J. Bickley, H. Bindslev[14], T. Bonicelli, S.J. Booth, G. Bosia, M. Botman, D. Boucher, P. Boucquey, P. Breger, H. Brelen, H. Brinkschulte, T. Brown, M. Brusati, T. Budd, M. Bures, T. Businaro, P. Butcher, H. Buttgereit, C. Caldwell-Nichols, D.J. Campbell, P. Card, G. Celentano, C.D. Challis, A.V.Chankin[23], D. Chiron, J. Christiansen, C. Christodoulopoulos, P. Chuilon, R. Claesen, S. Clement, E. Clipsham, J.P. Coad, M. Comiskey[4], S. Conroy, M. Cooke, S. Cooper, J.G. Cordey, W. Core, G. Corrigan, S. Corti, A.E. Costley, G. Cottrell, M. Cox[7], P. Cripwell, H. de Blank[15], H. de Esch, L. de Kock, E. Deksnis, G.B. Denne-Hinnov, G. Deschamps, K.J. Dietz, S.L. Dmitrenko, J. Dobbing, N. Dolgetta, S.E. Dorling, P.G. Doyle, D.F. Düchs, H. Duquenoy, A. Edwards, J. Ehrenberg, A. Ekedahl, T. Elevant[11], S.K. Erents[7], L.G. Eriksson, H. Fajemirokun[12], H. Falter, D. Flory, J. Freiling[15], C. Froger, P. Froissard, K. Fullard, M. Gadeberg, A. Galetsas, D. Gambier, M. Garribba, P. Gaze, R. Giannella, A. Gibson, R.D. Gill, A. Girard, A. Gondhalekar, C. Gormezano, N.A. Gottardi, C. Gowers, B.J. Green, R. Haange, G Haas, A. Haigh, G. Hammett[6], C.J. Hancock, P.J. Harbour, N.C. Hawkes[7], P. Haynes[7], J.L. Hemmerich, T. Hender[7], F.B. Herzog, R.F. Herzog, J. Hoekzema, J. How, M. Huart, L Hughes, T.P. Hughes[4], M. Hugon, M. Huguet, A. Hwang[7], B. Ingram, M. Irving, J. Jacquinot, H. Jaeckel, J.F. Jaeger, G. Janeschitz[13], S. Jankowicz[22], O.N. Jarvis, F. Jensen, E.M. Jones, L.P.D.F. Jones, T.T.C. Jones, J-F. Junger, E. Junique, A. Kaye, B.E. Keen, M. Keilhacker, G.J. Kelly, W. Kerner, R. Konig, A. Konstantellos, M. Kovanen[20], G. Kramer[15], P. Kupschus, R. Lässer, J.R. Last, B. Laundy, L. Lauro-Taroni, K. Lawson[7], M. Lennholm, A. Loarte, R. Lobel, P. Lomas, M. Loughlin, C. Lowry, B. Macklin, G. Maddison[7], G. Magyar, W. Mandl[13], V. Marchese, F. Marcus, J. Mart, E. Martin, R. Martin-Solis[8], P. Massmann, G. McCracken[7], P. Meriguet, P. Miele, S.F. Mills, P. Millward, R. Mohanti[17], P.L. Mondino, A. Montvai[3], S. Moriyama[28], P. Morgan, H. Morsi, G. Murphy, M. Mynarends, R. Myrnäs[16], C. Nardone, F. Nave[21], G. Newbert, M. Newman, P. Nielsen, P. Noll, W. Obert, D. O'Brien, J. O'Rourke, R. Ostrom, M. Ottaviani, M. Pain, F. Paoletti, S. Papastergiou, D. Pasini, A. Peacock, N. Peacock[7], D. Pearson[12], R. Pepe de Silva, G. Perinic, C. Perry, M. Pick, R. Pitts[7], J. Plancoulaine, J-P. Poffé, F. Porcelli, L. Porte[19], R. Prentice, S. Puppin, S. Putvinsko[23], G. Radford[9], T. Raimondi, M.C. Ramos de Andrade, P-H. Rebut, R. Reichle, E. Righi, F. Rimini, D. Robinson[7], A. Rolfe, R.T. Ross, L. Rossi, R. Russ, P. Rutter, H.C. Sack, G. Sadler, G. Saibene, J.L. Salanave, G. Sanazzaro, A. Santagiustina, R. Sartori, C. Sborchia, P. Schild, M. Schmid, G. Schmidt[6], B. Schunke, S.M. Scott, A. Sibley, R. Simonini, A.C.C. Sips, P. Smeulders, R. Stankiewicz[27], M. Stamp, P. Stangeby[18], D.F. Start, C.A. Steed, D. Stork, P.E. Stott, T.E. Stringer, P. Stubberfield, D. Summers, H. Summers[19], L. Svensson, J.A. Tagle[21], A. Tanga, A. Taroni, A. Tesini, P.R. Thomas, E. Thompson, K. Thomsen, J.M. Todd, P. Trevalion, B. Tubbing, F. Tibone, E. Usselmann, H. van der Beken, G. Vlases, M. von Hellermann, T. Wade, C. Walker, R. Walton[6], D. Ward, M.L. Watkins, M.J. Watson, S. Weber[10], J. Wesson, T.J. Wijnands, J. Wilks, D. Wilson, T. Winkel, R. Wolf, B. Wolle[24], D. Wong, C. Woodward, Y. Wu[25], M. Wykes, I.D. Young, L. Zannelli, Y. Zhu[26], W. Zwingmann.

PERMANENT ADDRESSES

1. UKAEA, Harwell, Didcot, Oxon, UK.
2. University of Leicester, Leicester, UK.
3. Central Research Institute for Physics, Academy of Sciences, Budapest, Hungary.
4. University of Essex, Colchester, UK.
5. ENEA-CNR, Padova, Italy.
6. Princeton Plasma Physics Laboratory, New Jersey, USA.
7. UKAEA Culham Laboratory, Abingdon, Oxon, UK.
8. Universidad Complutense de Madrid, Spain.
9. Institute of Mathematics, University of Oxford, UK.
10. Freien Universität, Berlin, F.R.G.
11. Swedish Energy Research Commission, S-10072 Stockholm, Sweden.
12. Imperial College of Science and Technology, University of London, UK.
13. Max Planck Institut für Plasmaphysik, Garching bei München, FRG.
14. Risø National Laboratory, Denmark.
15. FOM Instituut voor Plasmafysica, 3430 Be Nieuwegein, The Netherlands.
16. University of Lund, Sweden.
17. North Carolina State University, Raleigh, NC, USA
18. Institute for Aerospace Studies, University of Toronto, Downsview, Ontario, Canada.
19. University of Strathclyde, 107 Rottenrow, Glasgow, UK.
20. Nuclear Engineering Laboratory, Lapeenranta University, Finland.
21. CIEMAT, Madrid, Spain.
22. Institute for Nuclear Studies, Otwock-Swierk, Poland.
23. Kurchatov Institute of Atomic Energy, Moscow, USSR
24. University of Heidelberg, Heidelberg, FRG.
25. Institute for Mechanics, Academia Sinica, Beijing, P.R. China.
26. Southwestern University of Physics, Leshan, P.R. China.
27. RCC Cyfronet, Otwock Swierk, Poland.
28. JAERI, Naka Fusion Research Establishment, Ibaraki, Japan.
29. ENEA, Frascati, Italy.

At 1st June 1991